

CHAPTER 12

IMAGE REGISTRATION

Recent advances in medical imaging have made it possible to obtain three-dimensional (3-D) anatomical and metabolic information about the internal structure of the human body. As described in Chapters 4–7, different medical imaging modalities provide specific information about human physiology and physiological processes that is often complementary in diagnosis. To better understand physiological processes, images obtained from different modalities need to be registered. For example, anatomical images of the brain obtained from magnetic resonance imaging (MRI) modality need to be registered with metabolic images of the same brain obtained from the positron emission tomography (PET) imaging modality to analyze the metabolism within the anatomical volume of a tumor. Through the comparative quantitative and qualitative analyses of anatomical and metabolic volumes of the tumor from the registered images acquired during the treatment, the response of the treatment can be evaluated. Analysis of registered 3-D multimodality images from a control group of subjects allows the study of variance of specific features for better diagnosis, understanding of pathology, and therapeutic intervention protocols. In addition, postprocessing registration methods are useful in image-guided surgery, functional mapping, and characterization of normal versus abnormal physiological processes.

To study the variability of anatomical and functional (or metabolic) structures among the subjects, images from respective modalities can be registered to develop computerized atlases. The atlases can be broadly classified into two categories: structural computerized atlas (SCA) and functional computerized atlas (FCA). The SCA representing the anatomical variations among subjects can be developed using registered images from anatomical medical imaging modalities such as computer tomography (CT) or conventional MRI. It can be used as models for image segmentation and extraction of a structural volume of interest (VOI). It can also provide anatomical signatures for various groups of subjects for radiological studies. The FCA representing the metabolic variations among subjects for a specific pathology or function can be developed using registered images from functional medical imaging modalities such as functional MRI (fMRI), SPECT, or PET. When registered with structural images, it can be used to understand the metabolism or functional activity in a specific structural VOI. For example, the metabolism of a specific structural VOI of the brain can be studied to evaluate the cognitive functions of a subject. Figure 12.1 shows a schematic diagram of multimodality MR–PET medical

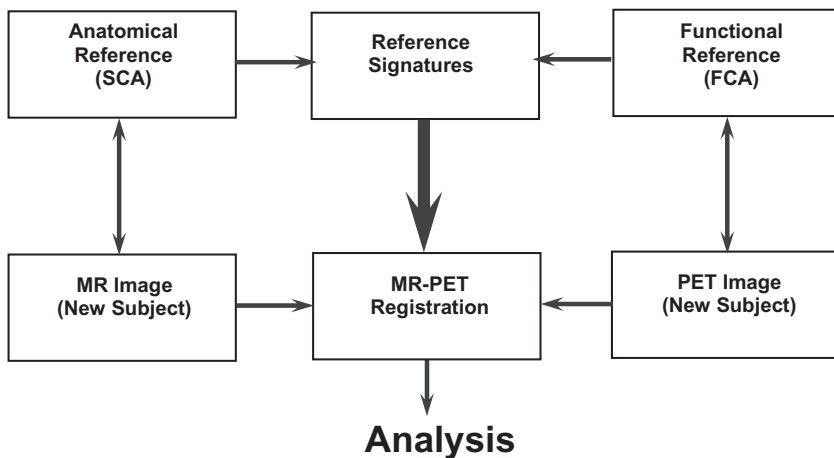


Figure 12.1 A schematic diagram of multimodality MR–PET image analysis using computerized atlases.

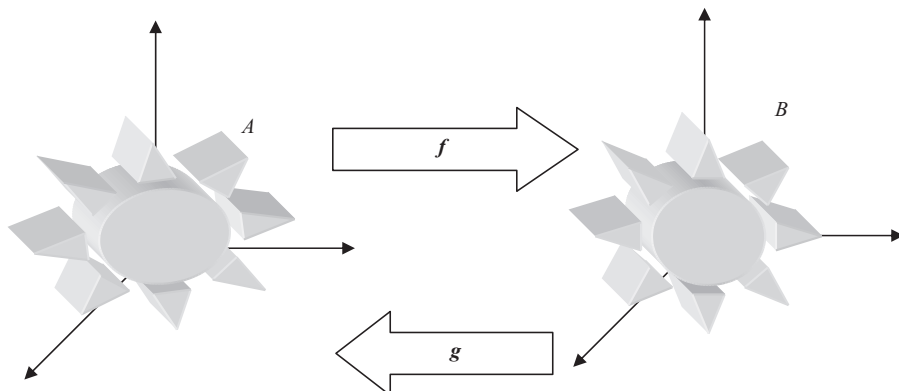


Figure 12.2 Image registration through transformation.

image analysis using the SCA and FCA. Anatomical and functional references are obtained using the SCA and FCA, respectively, for a specific physiological region such as the brain. The MR and PET brain images of a patient are then registered and analyzed in the context of the respective reference signature obtained from the atlases. As mentioned above, the atlases provide variability models for the analysis and interpretation of structural and functional images (1–6).

Image registration methods and algorithms provide transformation of a source image to the target image. The target image may be an image of the same or any other subject from any medical imaging modality. As described above, the target image could also be from an atlas. In ideal cases the transformation from source to target image should be reversible; that is, by using the inverse transformation, the source image can be recovered from the target image. Also, the transformation must preserve the topological properties of the image. Figure 12.2 shows a forward

transformation f to map the source image A to the target image B and a reverse transformation g for mapping the target image B to the source image A . In ideal cases, g is the inverse of f .

Although multimodality image registration and analysis methods can be applied to any physiological region, the methods in this chapter are described in the context of registration of human brain images. The registration of human brain images is a challenging problem in multimodality brain image analysis (1–35). However, references are provided for the registration of images of other physiological regions, such as the chest (36–40).

The approaches investigated in multimodality brain image registration and analysis can be divided into three broad categories.

1. External Markers and Stereotactic Frame-Based Landmark Registration:

The first category belongs to image registration and analysis methods, which require external markers in multiple scans or the use of stereotactic frames to establish a common coordinate system (1–3, 7–9). Stereotactic methods using special frames with markers, which are visible in different modalities, have also been used for image registration (1–9). Such external landmark-based registration methods are based on coordinate transformation (rotation, translation, and scaling) and interpolation computed from visible markers (21) by optimizing the mean squared error. Stereotactic frames are usually uncomfortable for the patient.

2. Rigid-Body Transformation-Based Global Registration: The second category of multimodality image registration methods treats the brain volume as a rigid body for global registration. Levy et al. presented a principal axes transformation-based 3-D registration method, which requires no operator interaction (11–15). This method was used in PET-PET (11), MR-MR (14) and MR-PET (15) brain image registration. PET scans, because of their limited field of view, often do not cover the entire brain, while MR scans are usually obtained for the entire brain volume. In such cases, the PET volume does not match the MR volume. The principal axes transformation method therefore does not provide accurate registration of MR and PET volumes. An iterative principle axes registration method was developed by Dhawan et al. to register MR brain images with PET scans covering the partial volume of the brain (15).

3. Image Feature-Based Registration: A large number of algorithms have been developed for image registration based on image features involving edges, contours, surfaces, volumes, and internal landmarks (16–35). This category can be divided into two major subcategories.

a. Boundary and Surface Matching-Based Registration: Image registration methods have been developed using edges, boundary, and surface information from images (16–20). Pelizzari et al. presented a surface matching-based registration method that maps a large number of points through a computer (16, 17). In this surface matching technique, 3-D models of the surface to be matched are first produced by outlining contours on

serial slices of each scan. The surface or boundary matching methods may require extensive computation and often need operator interaction to guide a nonlinear optimization. With CT or MR scans, the identification of the external surface is usually not a problem. Pelizzari et al. (16) suggested the use of PET transmission scans to identify the external surface from the PET data. 3-D models of the brain surface from both scans are then corrected for possible geometrical errors. A geometric transformation is obtained by minimizing a predefined error function between the surfaces. Once the transformation is determined through surface matching, the registration information is transferred between the scans using the VOI solid model constructed from its boundary contours (16–20).

- b. Image Landmarks and Feature-Based Registration:** Recently, several image registration algorithms have been developed that utilize predefined anatomical landmarks or features that can be identified and extracted in images (23–35). Bayesian model-based probabilistic methods have been used to integrate 3-D image information for registration (23, 24). Neuroanatomical atlases have been used for elastic matching of brain images (25–30). Rohr et al. used a landmark-based elastic matching algorithm for image registration (34). Other probabilistic model-based approaches, such as maximum likelihood estimation, have been investigated in the literature (20, 35).

12.1. RIGID-BODY TRANSFORMATION

Rigid-body transformation is primarily based on translation and rotation operations. Two images of equal dimensions are registered by applying a pixel-by-pixel transformation consistently throughout the image space. In three dimensions, a rigid transformation-based mapping of a point vector \mathbf{x} to \mathbf{x}' is defined by

$$\mathbf{x}' = \mathbf{R}\mathbf{x} + \mathbf{t} \quad (12.1)$$

where \mathbf{R} is a rotation matrix and \mathbf{t} is translation vector.

The translation and rotation operations in individual dimensions of the 3-D coordinate space are shown in Figure 12.3 and can be expressed as

- a.** Translation along x -axis by p :

$$\begin{aligned} x' &= x + p \\ y' &= y \\ z' &= z \end{aligned} \quad (12.2)$$

- b.** Translation along y -axis by q :

$$\begin{aligned} x' &= x \\ y' &= y + q \\ z' &= z \end{aligned} \quad (12.3)$$

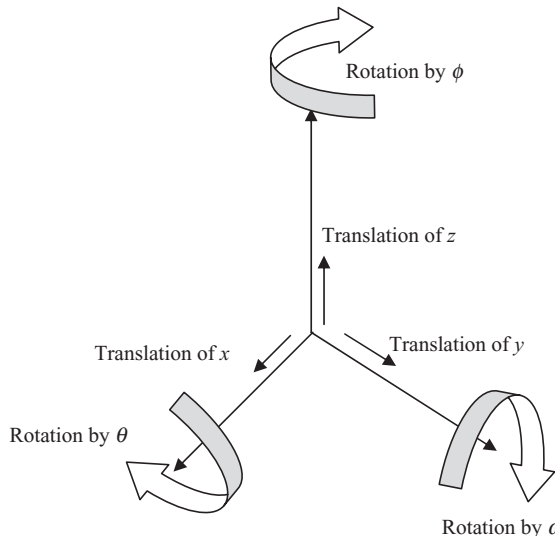


Figure 12.3 The translation and rotation operations of a 3-D rigid transformation.

c. Translation along z -axis by r :

$$\begin{aligned}x' &= x \\y' &= y \\z' &= z + r\end{aligned}\tag{12.4}$$

d. Rotation about x -axis by θ :

$$\begin{aligned}x' &= x \\y' &= y \cos \theta + z \sin \theta \\z' &= -y \sin \theta + z \cos \theta\end{aligned}\tag{12.5}$$

e. Rotation about y -axis by ω :

$$\begin{aligned}x' &= x \cos \omega - z \sin \omega \\y' &= y \\z' &= x \sin \omega + z \cos \omega\end{aligned}\tag{12.6}$$

f. Rotation about z -axis by ϕ :

$$\begin{aligned}x' &= x \cos \phi + y \sin \phi \\y' &= -x \sin \phi + y \cos \phi \\z' &= z\end{aligned}\tag{12.7}$$

It should be noted that the order of operations in the translation and rotation operations is important. Different results could be obtained if the order of translation and rotation operations is changed.

It can be shown that the rotation matrix \mathbf{R} for the x - y - z rotational order of operation can be given as

$$\mathbf{R} = R_\theta R_\omega R_\phi = \begin{bmatrix} \cos\theta & \sin\theta & 0 \\ -\sin\theta & \cos\theta & 0 \\ 0 & 0 & 1 \end{bmatrix} \begin{bmatrix} \cos\omega & 0 & -\sin\omega \\ 0 & 1 & 0 \\ \sin\omega & 0 & \cos\omega \end{bmatrix} \begin{bmatrix} 1 & 0 & 0 \\ 0 & \cos\phi & \sin\phi \\ 0 & -\sin\phi & \cos\phi \end{bmatrix} \quad (12.8)$$

12.1.1 Affine Transformation

Affine transformation is a special case of rigid-body transformation that includes translation, rotation, and scaling operations. If the two image volumes to be registered are not at the same scale, a scaling parameter in each dimension has to be added as

$$\begin{aligned} x' &= ax \\ y' &= by \\ z' &= cz \end{aligned} \quad (12.9)$$

where a , b , and c are the scaling parameters along x -, y -, and z -directions.

The affine transformation can be expressed as:

$$\mathbf{x}' = \mathbf{Ax} \quad (12.10)$$

where \mathbf{A} is the affine matrix that includes the translation, rotation, and scaling transformation with nine parameters.

Thus, the overall mapping can be expressed as

$$\begin{bmatrix} x' \\ y' \\ z' \\ 1 \end{bmatrix} = \begin{bmatrix} 1 & 0 & 0 & p \\ 0 & 1 & 0 & q \\ 0 & 0 & 1 & r \\ 0 & 0 & 0 & 1 \end{bmatrix} \begin{bmatrix} \cos\theta & \sin\theta & 0 & 0 \\ -\sin\theta & \cos\theta & 0 & 0 \\ 0 & 0 & 1 & 0 \\ 0 & 0 & 0 & 1 \end{bmatrix} \begin{bmatrix} \cos\omega & 0 & -\sin\omega & 0 \\ 0 & 1 & 0 & 0 \\ \sin\omega & 0 & \cos\omega & 0 \\ 0 & 0 & 0 & 1 \end{bmatrix} \begin{bmatrix} 1 & 0 & 0 & 0 \\ 0 & \cos\phi & \sin\phi & 0 \\ 0 & -\sin\phi & \cos\phi & 0 \\ 0 & 0 & 0 & 1 \end{bmatrix} \begin{bmatrix} x \\ y \\ z \\ 1 \end{bmatrix} \quad (12.11)$$

12.2. PRINCIPAL AXES REGISTRATION

Principal axes registration (PAR) can be used for global matching of two binary volumes such as segmented brain volumes from CT, MR, or PET images (11–15). Let us represent a binary segmented $B(x, y, z)$ as

$$\begin{aligned} B(x, y, z) &= 1 \text{ if } (x, y, z) \text{ is in the object} \\ &= 0 \text{ if } (x, y, z) \text{ is not in the object.} \end{aligned} \quad (12.12)$$

Let the centroid of the binary volume $B(x, y, z)$ be represented by (x_g, y_g, z_g) where

$$\begin{aligned} x_g &= \frac{\sum_{x,y,z} xB(x, y, z)}{\sum_{x,y,z} B(x, y, z)} \\ y_g &= \frac{\sum_{x,y,z} yB(x, y, z)}{\sum_{x,y,z} B(x, y, z)} \\ z_g &= \frac{\sum_{x,y,z} zB(x, y, z)}{\sum_{x,y,z} B(x, y, z)}. \end{aligned} \quad (12.13)$$

Following Goldstein (22), the principle axes of $B(x, y, z)$ are the eigenvectors of the inertia matrix I :

$$I = \begin{bmatrix} I_{xx} & -I_{xy} & -I_{xz} \\ -I_{yx} & I_{yy} & -I_{yz} \\ -I_{zx} & -I_{zy} & I_{zz} \end{bmatrix}$$

where

$$\begin{aligned} I_{xx} &= \sum_{x,y,z} [(y - y_g)^2 + (z - z_g)^2] B(x, y, z) \\ I_{yy} &= \sum_{x,y,z} [(x - x_g)^2 + (z - z_g)^2] B(x, y, z) \\ I_{zz} &= \sum_{x,y,z} [(x - x_g)^2 + (y - y_g)^2] B(x, y, z) \\ I_{xy} = I_{yx} &= \sum_{x,y,z} (x - x_g)(y - y_g) B(x, y, z) \\ I_{xz} = I_{zx} &= \sum_{x,y,z} (x - x_g)(z - z_g) B(x, y, z) \\ I_{yz} = I_{zy} &= \sum_{x,y,z} (y - y_g)(z - z_g) B(x, y, z). \end{aligned} \quad (12.14)$$

The inertia matrix is diagonal when computed with respect to the principal axes. Thus, the centroid and the principal axes provide a method to completely describe the orientation of an arbitrary volume. The method can resolve six degrees of freedom of an object, including three rotations and three translations. Furthermore, it provides a precise way of comparing the orientations of two binary volumes through rotation, translation, and scaling.

Let us define a normalized eigenvector matrix E as

$$E = \begin{bmatrix} e_{11} & e_{12} & e_{13} \\ e_{21} & e_{22} & e_{23} \\ e_{31} & e_{32} & e_{33} \end{bmatrix}. \quad (12.15)$$

Let $\mathbf{R} = R_\alpha R_\beta R_\gamma$ represent the rotation matrix as

$$R_\alpha R_\beta R_\gamma = \begin{bmatrix} \cos \alpha & \sin \alpha & 0 \\ -\sin \alpha & \cos \alpha & 0 \\ 0 & 0 & 1 \end{bmatrix} \begin{bmatrix} \cos \beta & 0 & -\sin \beta \\ 0 & 1 & 0 \\ \sin \beta & 0 & \cos \beta \end{bmatrix} \begin{bmatrix} 1 & 0 & 0 \\ 0 & \cos \gamma & \sin \gamma \\ 0 & -\sin \gamma & \cos \gamma \end{bmatrix}. \quad (12.16)$$

where α , β , and γ are the rotation angles with respect to the x , y , and z axes, respectively.

By equating the normalized eigenvector matrix to the rotation matrix as

$$E = R_\alpha R_\beta R_\gamma. \quad (12.17)$$

It can be shown that

$$\begin{aligned} \beta &= \arcsin(e_{31}) \\ \alpha &= \arcsin(-e_{21}/\cos \beta) \\ \gamma &= \arcsin(-e_{32}/\cos \beta). \end{aligned} \quad (12.18)$$

Given two volumes, V_1 and V_2 , for registration, the PAR method provides the following operations:

1. Translate the centroid of V_1 to the origin.
2. Rotate the principal axes of V_1 to coincide with the x -, y -, and z -axes.
3. Rotate the x , y , and z axes to coincide with the principal axes of V_2 .
4. Translate the origin to the centroid of V_2 .

Finally, the volume V_2 is scaled to match the volume V_1 using the scaling factor F_s

$$F_s = \sqrt[3]{\frac{V_1}{V_2}}. \quad (12.19)$$

Probabilistic models can be constructed by counting the occurrence of a particular binary subvolume that is extracted from the registered volumes corresponding to various images. Let $M(x, y, z)$ be a function describing the model providing the spatial probability distribution of the subvolume, then

$$M(x, y, z) = \frac{1}{n} \sum_{i=1}^n S_i(x, y, z). \quad (12.20)$$

where n is the total number of data sets in the model and $S_i(x, y, z)$ is the i th subvolume.

Figure 12.4 shows a model of brain ventricles that is based on the frequency of occurrence in registered brain images of 22 normal subjects using the PAR method. This composite model provides a 3-D probabilistic spatial distribution of the ventricles. The probability of spatial matching as indicated by the gray-level value ranges from 0.0455 (1/22) to 1.0 (22/22). For visualization, an opacity factor equal to the probability of matching was assigned to all gray-level values (14). The consistency of the match of the third and fourth ventricles and the variability evident in the lateral ventricles can be noted in the rotated views of the model shown in Figure 12.5.

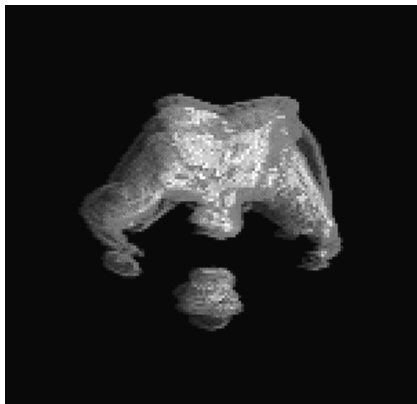


Figure 12.4 A 3-D model of brain ventricles obtained from registering 22 MR brain images using the PAR method.

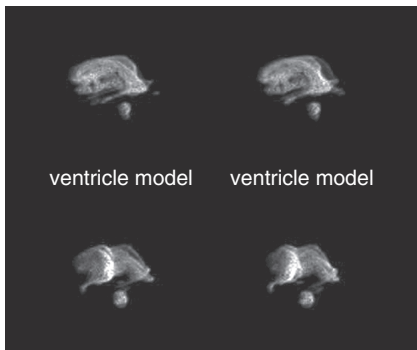


Figure 12.5 Rotated views of the 3-D brain ventricle model shown in Figure 12.3.

12.3. ITERATIVE PRINCIPAL AXES REGISTRATION

Dhawan et al. (15) developed an iterative PAR (IPAR) method for registering MR and PET brain images. The advantage of the IPAR over the conventional principal axes registration method is that the IPAR method can be used with partial volumes. This procedure assumes that the field of view (FOV) of a functional image such as PET is less than the full brain volume, while the other volume (MR image) covers the entire brain.

Let V_1 and V_2 represent two volumes to be registered. The IPAR method can be implemented using the following steps (15):

1. Find the full dynamic range of the PET data and select a threshold, T , which is about 20% of the maximum gray-level value. Threshold each PET slice to avoid streaking artifacts and overestimation of the brain regions, such that all pixels with gray-level values equal to or less than the threshold T are set to zero. Extract binary brain regions using a region-growing method on the thresholded PET slice data.

2. Threshold and extract binary brain regions from the MR data using a region-growing method.
3. Stack two-dimensional (2-D) binary segmented MR slices and interpolate as necessary to obtain cubic voxel dimensions using a shape-based interpolation algorithm (21). This is referred to as 3-D binary MR data.
4. Stack 2-D binary segmented PET slices and interpolate as necessary to obtain a cubic voxel dimension to match the voxel dimension of binary MR data using a shape-based interpolation algorithm (21). This is referred to as 3-D binary PET data.
5. Define a FOV box, $\text{FOV}(0)$, as a parallelepiped from the slices of the interpolated binary PET data to cover the PET brain volume. Because of the smaller FOV of the PET scanner, voxels outside the binary PET brain volume will have zero values.
6. Compute the centroid and principal axes of the binary PET brain volume as described above.
7. Add n slices to the $\text{FOV}(0)$ box (of binary PET brain volume) on the top and the bottom such that the augmented $\text{FOV}(n)$ box will have the same number of slices as the binary MR data. The added slices are spaced equally on the top and bottom. The $\text{FOV}(n)$ box will now be shrunk gradually back to its original size, $\text{FOV}(0)$, through an iterative process. Initially, the whole MR brain volume is used in computing the transformation parameters using the augmented $\text{FOV}(n)$ box. In each iteration, the $\text{FOV}(n)$ box is reduced in size and the binary MR data is trimmed accordingly to provide the current MR brain volume. This volume is used to compute the centroid and principal axes parameters to obtain a new transformation for matching the PET FOV box to the current MR brain. The iterative process continues until the FOV box reaches its original size to provide the final transformation parameters to register MR and PET data. Figure 12.6 shows three iterations of the IPAR algorithm for registration of two volumes. The IPAR algorithm is as follows.

For $i = n$ to 0:

- A. Compute the centroid and principal axes of the current binary MR brain volume. This binary MR brain volume is gradually trimmed at each step by the transformed $\text{FOV}(i)$ box.
- B. Transform the augmented $\text{FOV}(i)$ box according to the space of the MR slices as follows.

Let c_{PET} and c_{MR} be the centroids, (x_g, y_g, z_g) , of the binary PET and MR data, and let E_{PET} and E_{MR} be the normalized eigenvector matrices of the binary PET and MR data; then for any point, x_{PET} , its position, x_{MR} , in the MR space can be calculated as

$$x_{\text{MR}} = (E_{\text{MR}} E_{\text{PET}}^T (x_{\text{PET}} - c_{\text{PET}})) + c_{\text{MR}}. \quad (12.21)$$

The normalized eigenvector matrix of a binary volume will rotate the standard x -, y -, and z -axes parallel to the principal axes of the volume. If the centroid of the volume is first translated to the origin, then after rotation

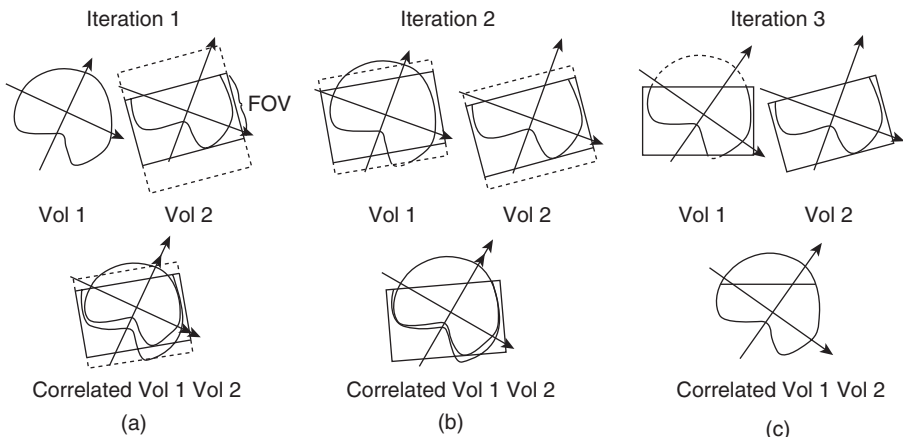


Figure 12.6 Three successive iterations of the IPAR algorithms for registration of vol 1 and vol 2: The results of the first iteration (a), the second iteration (b), and the final iteration (c). Vol 1 represents the MR data while the PET image with limited field of view (FOV) is represented by vol 2.

by the eigenvector matrix the x -, y -, and z -axes will be coincident with the principal axes of the volume.

The PET data is registered with the MR data through the process of the required translations and rotations. The rotation angles are determined as described above. To express all points, $(x_{PET}, y_{PET}, z_{PET})$, of the PET data in the coordinate space of the MR data, the following steps must be performed:

1. Translate the centroid of the binary PET data to the origin.
 2. Rotate the principal axes of the binary PET data to coincide with the x -, y -, and z -axes.
 3. Rotate the x -, y -, and z -axes to coincide with the MR principal axes.
 4. Translate the origin to the centroid of the binary MR data.
- C. Remove all voxels of the binary MR brain that lie outside the transformed $FOV(i)$ box. This is the new binary MR brain volume.

The final transformation parameters for registration of MR and PET data are obtained from the last iteration.

8. Interpolate the gray-level PET data to match the resolution of MR data, to prepare the PET data for registration with MR data.
9. Transform the gray-level PET data into the space of the MR slices using the last set of MR and PET centroids and principal axes. Extract the slices from the transformed gray-level PET data that match the gray-level MR image.

The IPAR algorithm allows registration of two 3-D image data sets, in which one set does not cover the entire volume but has the subvolume contained in the other data set. Figures 12.7 a–c show the MR (middle rows) and PET (bottom rows) brain

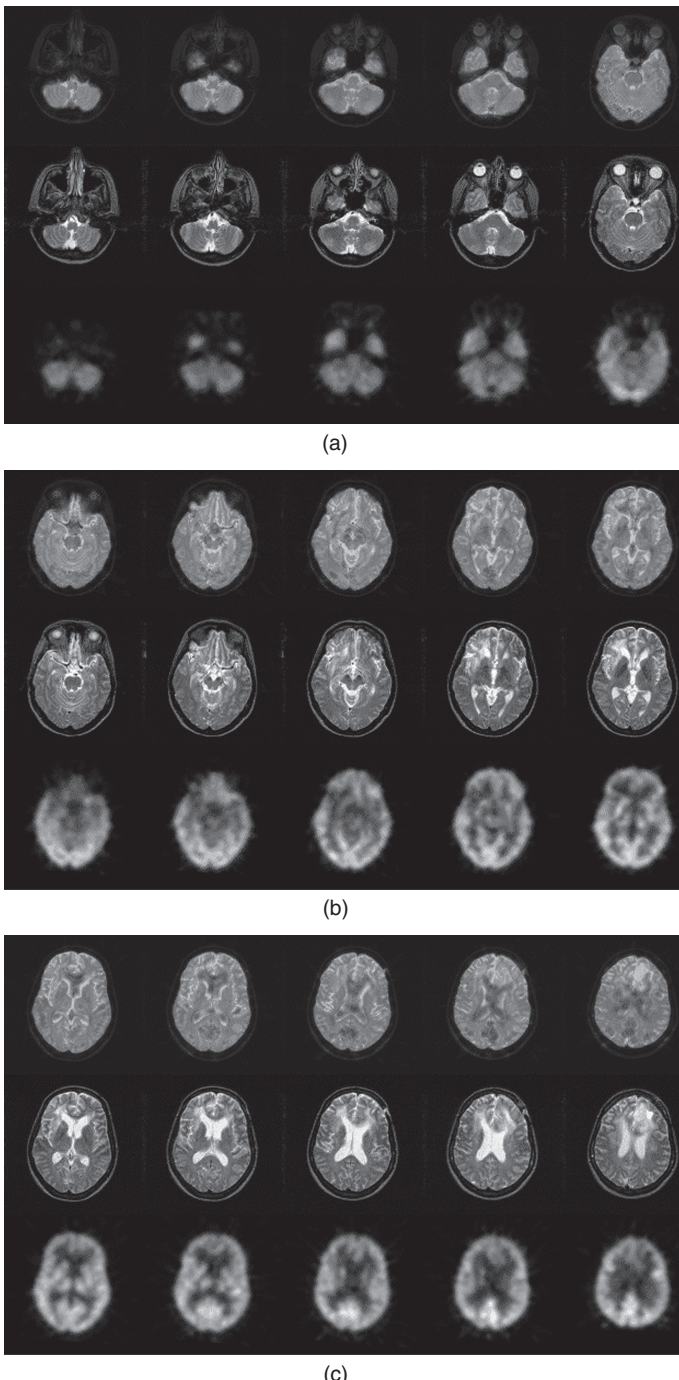


Figure 12.7 (a, b, c) Sequential slices of MR (middle rows) and PET (bottom rows) and the registered MR–PET brain images (top row) of the corresponding slices using the IPAR method.

images of a patient with a brain tumor. The 3-D MR and PET images were registered using the IPAR method. The corresponding registered overlaid MR–PET images for the respective slices are shown in the top rows. The MR data was obtained from a Philips Gyroscan S15 scanner with 256×256 pixel resolution corresponding to about 0.9 mm pixel size with an interslice separation of 5 mm. The PET data was obtained from a Siemens-CTI: 951 scanner as 128×128 pixel images with a pixel size of 1.9 mm. The interslice distance of the PET data was about 3.5 mm. The PET brain FOV was about 70% of the MR brain FOV.

12.4. IMAGE LANDMARKS AND FEATURES-BASED REGISTRATION

Rigid and nonrigid transformations have been used in image landmarks (points) and features-based medical image registration (16–20). Once the corresponding landmarks or features are identified from source and target image spaces, a customized transformation can be computed for registering the source image into the target image space. In the previous sections, global registration methods (PAR and IPAR) based on principal axes were described. These methods use the basic principle of rigid-body transformation with an additional operation of scaling. However, a number of nonrigid transformation methods that exploit the relationships of corresponding points and features such as surfaces in source and target images have been investigated for registration (16–20). Two simple algorithms for point-based registration of source and target images are described below.

12.4.1 Similarity Transformation for Point-Based Registration

Let us assume that \mathbf{x} and \mathbf{y} are, respectively, the corresponding points (represented as vectors) in the source and target image spaces belonging to the source X and target Y images. A nonrigid transformation $T(\mathbf{x})$ for registering the source image into the target image space can be defined by a combination of rotation, translation, and scaling operations to provide \mathbf{x}' from \mathbf{x} as (41)

$$\mathbf{x}' = \mathbf{srx} + \mathbf{t} \quad (12.22)$$

such that the registration error E is minimized as

$$E(\mathbf{x}) = T(\mathbf{x}) - \mathbf{y} \quad (12.23)$$

where \mathbf{r} , \mathbf{s} , and \mathbf{t} represent the rotation, scaling, and translation operations.

A transformation should be obtained with \mathbf{r} , \mathbf{s} , and \mathbf{t} values to minimize the error function as

$$\sum_{i=1}^N w_i^2 |srx_i + t - y_i|^2 \quad (12.24)$$

where w_i are the weighting factors representing the confidence in the specific landmark (point) or feature correspondence and N is the total number of landmarks.

The following algorithm can be implemented to register the source image into the target image space:

1. Set $s = 1$.
2. Find \mathbf{r} through the following steps:
 - (a) Compute the weighted centroid of the body representing the set of landmarks (points) in each space as

$$\bar{\mathbf{x}} = \frac{\sum_{i=1}^N w_i^2 \mathbf{x}_i}{\sum_{i=1}^N w_i^2}$$

$$\bar{\mathbf{y}} = \frac{\sum_{i=1}^N w_i^2 \mathbf{y}_i}{\sum_{i=1}^N w_i^2} \quad (12.25)$$

- (b) Compute the distance of each landmark from the centroid as

$$\bar{\mathbf{x}}_i = \mathbf{x}_i - \bar{\mathbf{x}}$$

$$\bar{\mathbf{y}}_i = \mathbf{y}_i - \bar{\mathbf{y}} \quad (12.26)$$

- (c) Compute the weighted covariance matrix as

$$\mathbf{Z} = \sum_{i=1}^N w_i^2 \bar{\mathbf{x}}_i \bar{\mathbf{y}}_i^t \quad (12.27)$$

with a singular value decomposition as

$$\mathbf{Z} = \mathbf{U} \Lambda \mathbf{V}^t$$

where $\mathbf{U}' \mathbf{U} = \mathbf{V}' \mathbf{V} = \mathbf{I}$

and

$$\Lambda = \text{diag}(\lambda_1, \lambda_2, \lambda_3); \quad \lambda_1 \geq \lambda_2 \geq \lambda_3 \geq 0 \quad (12.28)$$

- (d) Compute $\mathbf{r} = \mathbf{V} \text{diag}(1, 1, \det(\mathbf{V}\mathbf{U})) \mathbf{U}^t$ (12.29)

3. Compute the scaling factor

$$s = \frac{\sum_{i=1}^N w_i^2 \mathbf{r} \bar{\mathbf{x}}_i \cdot \bar{\mathbf{y}}_i}{\sum_{i=1}^N w_i^2 \mathbf{r} \bar{\mathbf{x}}_i \cdot \bar{\mathbf{x}}_i} \quad (12.30)$$

4. Compute $\mathbf{t} = \bar{\mathbf{y}} - s \mathbf{r} \bar{\mathbf{x}}$ (12.31)

12.4.2 Weighted Features-Based Registration

Different optimization functions can be designed to improve the computation of parameters of transformation for registration of the source image into the target

image space. In the above example, an error function was used for minimization to achieve the transformation parameters. In many registration methods, geometrical features or landmarks are used to register 3-D images. Defining a transformation T on \mathbf{x} as in Equation 12.23, a disparity function can be designed as

$$d(T) = \sqrt{\sum_{i=1}^{N_s} \sum_{j=1}^{N_{X_i}} w_{ij}^2 \|T(\mathbf{x}_{ij}) - \mathbf{y}_{ij}\|^2} \quad (12.32)$$

where $\{X_i\}$ for $i = 1, 2, 3, \dots, N_s$ represents a set of corresponding data shapes in \mathbf{x} and \mathbf{y} spaces.

The transformation T must minimize the disparity function to register the source image into the target image space utilizing the correspondence of geometrical features.

An iterative algorithm can be implemented for registration as (42);

1. Determine the parameters for a rigid or nonrigid-body transformation T using the above algorithm in Section 12.4.1.
2. Initialize the transformation optimization loop for $k = 1$ as

$$\begin{aligned} \mathbf{x}_{ij}^{(0)} &= \mathbf{x}_{ij} \\ \mathbf{x}_{ij}^{(1)} &= T^{(0)}(\mathbf{x}_{ij}^{(0)}) \end{aligned} \quad (12.33)$$

3. For each shape X_i in the source space, find the closest points in the corresponding shape in the target space Y_i as

$$\mathbf{y}_{ij}^{(k)} = C_i(\mathbf{x}_{ij}^{(k)}, Y_i); \quad j = 1, 2, 3, \dots, N_{x_i} \quad (12.34)$$

where C_i is the corresponding function.

4. Compute the transformation between $\{\mathbf{x}_{ij}^{(0)}\}$ and $\{\mathbf{y}_{ij}^{(k)}\}$ using the weights $\{w_{ij}\}$ using the above algorithm in Section 12.4.1.
5. Use the transformation parameters for registration of the corresponding points as

$$\mathbf{x}_{ij}^{(k+1)} = T^{(k)}(\mathbf{x}_{ij}^{(0)}) \quad (12.35)$$

6. Compute the disparity measure difference $d(T^{(k)}) - d(T^{(k+1)})$. If the convergence criterion is met, stop; otherwise increment k and go to step 3 for next iteration.

12.5. ELASTIC DEFORMATION-BASED REGISTRATION

Elastic deformation methods mimic a manual registration process. In the registration process, one of the two volumes is considered to be made of elastic material while the other volume serves as a rigid reference. The purpose of elastic matching is to map the elastic volume to the reference volume. The elastic volume is deformed by applying external forces such that it matches the reference model. The matching process starts in a coarse mode in which large differences are corrected first. The

fine, detailed adjustments are the done later in the deformation-based mapping process. The process stops when an objective function based on the similarity measure is optimized.

There are several constraints that can be applied during the deformation for local matching. The constraints include smoothness and incompressibility. The smoothness constraint ensures that there is continuity in the deformed volume while the incompressibility constraint guarantees that there is no change in the total volume. The forces required to locally match the volumes of interest are calculated with these constraints and can be expressed by the general equation for motion of a deformable body in Lagrangian form as

$$f(\mathbf{r}, t) = \mu \frac{\partial^2 \mathbf{r}}{\partial t^2} + \gamma \frac{\partial \mathbf{r}}{\partial t} + \frac{\partial \varepsilon(\mathbf{r})}{\partial \mathbf{r}} \quad (12.36)$$

where $f(\mathbf{r}, t)$ is the force acting on a particle at the position \mathbf{r} at time t , μ , and γ are, respectively, the mass and damping constant of the deformable body; and $\varepsilon(\mathbf{r})$ is the internal energy of deformation. For implementation, an image voxel can be treated as a particle for which a movement is calculated for image registration.

Let the elastic volume be represented by V_1 with the coordinate system $\mathbf{x} = (x_1, x_2, x_3)$ and the reference volume be represented by V_2 with the coordinate system $\mathbf{x}' = (x'_1, x'_2, x'_3)$. A relationship between the two coordinate systems can be expressed as

$$d\mathbf{r} = \frac{\partial \mathbf{r}}{\partial x_1} dx_1 + \frac{\partial \mathbf{r}}{\partial x_2} dx_2 + \frac{\partial \mathbf{r}}{\partial x_3} dx_3. \quad (12.37)$$

The partial differential operators on a position vector \mathbf{r} of a voxel in the registration space can be represented as

$$\vec{g}_i = \frac{\partial \mathbf{r}}{\partial x_i} \quad \text{for } i = 1, 2, 3. \quad (12.38)$$

Thus Equation 12.37 can be written as

$$d\mathbf{r} = \vec{g}_i dx_i. \quad (12.39)$$

Let \mathbf{u} be an arbitrary vector represented by (u_1, u_2, u_3) with respect to the coordinate system such that

$$\mathbf{u} = u_1 \vec{g}_1 + u_2 \vec{g}_2 + u_3 \vec{g}_3 \quad (12.40)$$

It can be shown that

$$\begin{aligned} u_i &= (u_j \vec{g}_j) \cdot \vec{g}_i = g_{ij} u_j \\ \text{with } g_{ij} &= \vec{g}_i \cdot \vec{g}_j \end{aligned} \quad (12.41)$$

where the quantities g_{ij} are components of the generalized metric tensor G_{ijk} in a 3-D coordinate system. The metric tensor G_{ijk} represents a distance measure with respect to a given coordinate system. Any transformation applied to the metric tensor generates a new metric tensor for the new coordinate system.

Thus, considering the position vector \mathbf{u} with respect to a point a (a_1, a_2, a_3) in the coordinate system, the metric tensor can be defined as

$$G_{ijk} = \int \frac{\partial \mathbf{u}}{\partial a_i} \frac{\partial \mathbf{u}}{\partial a_j} \frac{\partial \mathbf{u}}{\partial a_k}. \quad (12.42)$$

The metric tensor G_{ijk} can be considered the first-order derivative for the displacement field in the deformation process. A curvature tensor B_{ijk} can be defined to represent the second-order partial derivative form as

$$B_{ijk} = \int \frac{\partial^2 \mathbf{u}}{\partial a_i \partial a_j} \frac{\partial^2 \mathbf{u}}{\partial a_j \partial a_k} \frac{\partial^2 \mathbf{u}}{\partial a_k \partial a_i}. \quad (12.43)$$

The potential energy $\varepsilon(\mathbf{x})$ can be defined in terms of the metric tensor as

$$\varepsilon(\mathbf{x}) = k \sum_{ijk} (G_{ijk} - G_{ijk}^0)^2 \quad (12.44)$$

where G_{ijk}^0 is the resting metric tensor without any displacement field (undeformed situation) and k is a constant.

The elastic deformation function model can now be represented as

$$\varepsilon(\mathbf{r}) = \int_{\Omega} \|G_{ijk} - G_{ijk}^0\|^2 d\mathbf{u} \quad (12.45)$$

where Ω represents all voxels in the volume for registration.

A computational model for matching through elastic deformation can be formulated as a minimization problem of the cost function that is based on a similarity measure between the two volumes to be registered. Let $S(\mathbf{x}, \mathbf{x}')$ represent a similarity measure between the local region R centered at the location \mathbf{x} in V_1 and the region R' centered at \mathbf{x}' in V_2 . A displacement vector \mathbf{u} is defined as the difference between the two locations. The optimal match for R to the region R' for the displacement vector \mathbf{u} is the one that maximizes the similarity measure $S(\mathbf{x}, \mathbf{x}')$.

A possible form of the similarity measure can be expressed in terms of metric and curvature tensors as

$$S(\mathbf{x}, \mathbf{x}') = \int_{\Omega} \left(\|G_{ijk}^1 - G_{ijk}^2\|^2 + \|B_{ijk}^1 - B_{ijk}^2\|^2 \right) da_i da_j da_k \quad (12.46)$$

where the superscripts 1 and 2 represent, respectively, the deformable volume V_1 and the reference volume V_2 .

Alternately, the similarity measure $S(\mathbf{x}, \mathbf{x}')$ can be expressed in terms of differences in intensity levels or metric tensors. A cost function is defined to include the similarity measure and elastic constraints for regularization. The cost function guides the image matching process for computing the displacement vector for local regions. The optimization of the cost function provides the final mapping for image registration. For example, Christensen and Johnson (35) included a similarity measure based on the difference of intensity and a linear elastic operator L , applied on the displacement vector $\mathbf{u}(\mathbf{x})$ in the cost function $C(g_r, R, R')$ with a mapping transformation as

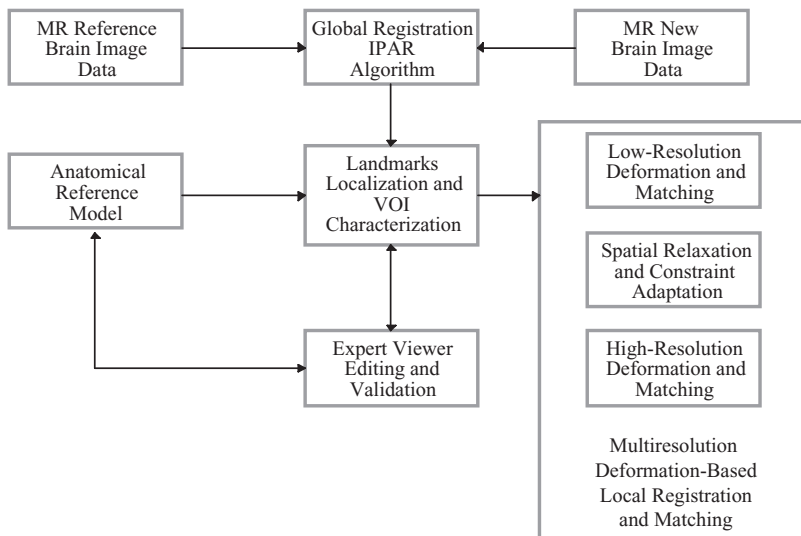


Figure 12.8 Block diagram for the MR image registration procedure.

$$C(g_r, R, R') = \int_{\Omega_R} |R(g_r(x) - R'(x)|^2 dx + \int_{\Omega_R} \|L_r u(x)\|^2 dx$$

with $L_r u(x) = -\alpha \nabla^2 u(x) - \beta \nabla(\nabla \cdot u(x)) + \gamma u(x)$ (12.47)

$$\text{where } \nabla = \left[\frac{\partial}{\partial x_1}, \frac{\partial}{\partial x_2}, \frac{\partial}{\partial x_3} \right] \text{ and } \nabla^2 = \left[\frac{\partial^2}{\partial x_1^2}, \frac{\partial^2}{\partial x_2^2}, \frac{\partial^2}{\partial x_3^2} \right]. \quad (12.48)$$

It can be noted that L_r is a differential operator that can cause the transformation to fold onto itself, destroying the topology. To avoid it, the Jacobian of the transformation is checked in each iteration to make sure that it is positive for all voxels in Ω_R , thus ensuring the preservation of topology.

As shown in Figure 12.8, for MR image registration, the MR-1 volume can be first registered with the MR-2 volume globally using the IPAR algorithm. The global registration improves the initial conditions for elastic deformation-based matching (36). Anatomical landmarks are then located from the globally registered volumes using an anatomical reference model with some topological knowledge of the respective anatomy. Thus, the whole 3-D volume can be localized into smaller volumes by choosing appropriate VOI. The VOI can be selected around the internal landmarks that are identified using the anatomical reference model. If necessary, user interaction may also be involved in the identification of the landmarks and related VOIs.

Once the VOIs are defined around internal landmarks, the VOIs of the elastic model are deformed through the application of external forces using a matching criterion that allows forces to change dynamically. The matching process, proceeding from coarse to fine mode, is repeated until the final match is achieved in the finest mode.

In brief, the local matching algorithm can be described as follows:

1. Perform a global registration of the two 3-D data sets using the IPAR or a manual landmark-based registration algorithm.
2. Compute a total similarity measure for the deformable volume V_1 and the reference volume V_2 from the globally registered 3-D data sets.
3. Identify internal landmarks using anatomical reference models to determine volumes of interests (VOI_is) where elastic deformation-based local registration is required.
4. For local registration:
 - a. Compute similarity measures and cost function for optimization.
 - b. If respective VOI_i are not similar,
 - c. Compute displacement vectors for voxels in the VOI_i as required for elastic deformation using the constrained optimization of the cost function.
 - d. Deform VOI_i of the deformable volume using the displacement vectors.
 - e. If deformed voxels are inconsistent with continuity or smoothness constraints, apply correction factors in the computation of displacement vectors and repeat step 4d.
 - f. If all VOI_is are processed and the cost function is minimized, end; otherwise go to step 4c.

5. Interpolate the entire deformed volume V_1 as required.
6. Compute the total similarity measure between the deformed volume V_1 and the reference volume V_2 .
7. If the total similarity measure between the deformed volume and the reference volume is improved, stop; otherwise check the internal landmarks and go to step 3.

Figure 12.9 shows the results of elastic deformation-based registration of 3-D MR brain images. The left column shows three target images of the 3-D MR brain data set considered as the reference volume V_2 . The middle column shows the images from the deformable volume V_1 . The right column shows the respective registered images through elastic deformation method. It can be seen from Figure 12.9 that the elastic deformation-based registration method provided reasonably good results. However, distortions at some of the corners of the registered images are evident. To address this problem, more emphasis on the continuity constraint and a better interpolation method are required.

Image registration and localized mapping remains an area of active research as the resolution of medical imaging improves to unveil high-resolution physiological structures. Multimodality image analysis with high-resolution structural mapping continues to provide a basis for understanding metabolic activities in anatomically referenced structures.

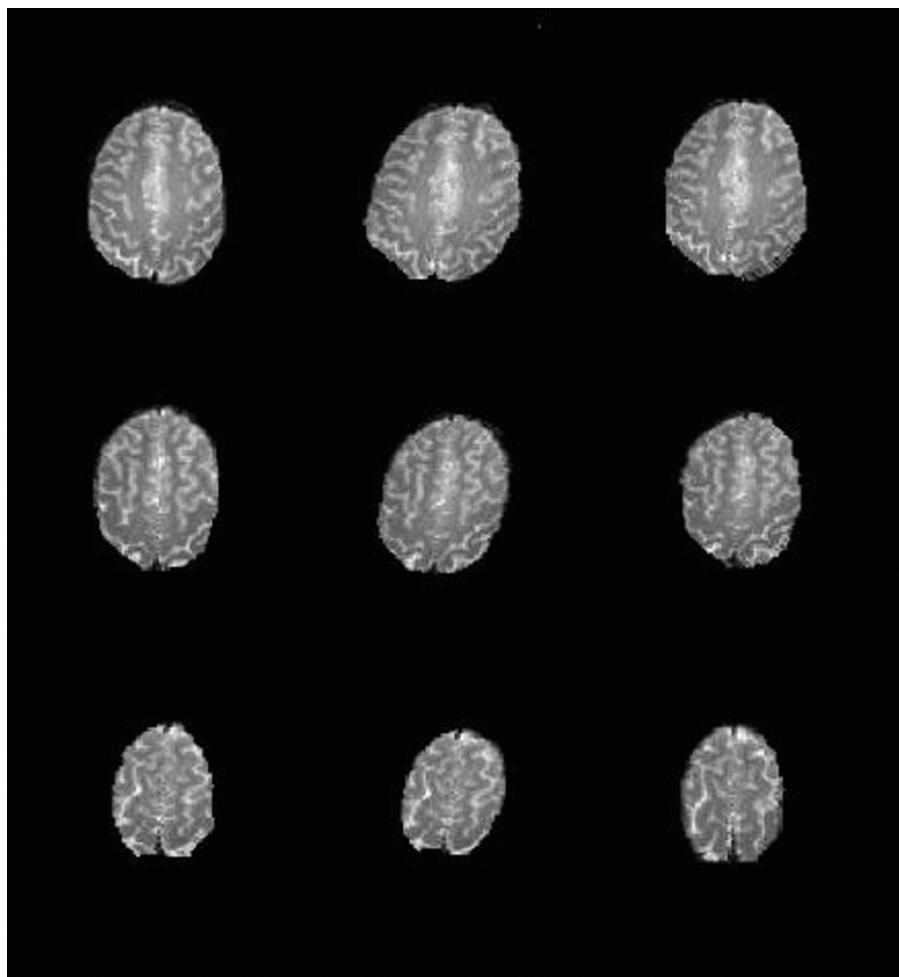


Figure 12.9 Results of the elastic deformation based registration of 3-D MR brain images: The left column shows three images of the reference volume; the middle column shows the respective images of the brain volume to be registered; and the right column shows the respective images of the registered brain volume.

12.6. EXERCISES

- 12.1. Define the problem of global registration of two volumes in medical imaging. Why is it important to refine global registration of multimodality medical images by local mapping and registration?
- 12.2. Describe the affine transformation for global image registration.
- 12.3. Derive mathematical expressions for the affine transformation for mapping the (x, y, z) coordinate system volume to the (x', y', z') coordinate system

- volume using at least using three different orders of operations. Are the final expressions same? If not, explain why.
- 12.4. How is a mapping relationship obtained from the eigenvalues of the rotation matrix?
 - 12.5. What are the basic differences between the rigid-body and elastic transformation-based approaches for image registration?
 - 12.6. Write and explain a mathematical expression for determining the displacement vector field for elastic deformation.
 - 12.7. What are the different approaches used for external and internal landmark-based image registration?
 - 12.8. In the MATLAB environment, extract CT images of the human brain. Using the distortion algorithm with rotation and scaling operations, obtain a second set of distorted CT images. Now use the original and distorted CT brain images for volume segmentation under the skull. Using the centroids and principal axes, apply the affine transformation to map-distorted images to the original brain images. Reslice the registered and original data sets for the three oblique cross-sections. Subtract the registered cross-section images from the respective original images to obtain residual images. Do residual images contain all zeros? Comment on the nonzero values of the residual images.
 - 12.9. Repeat Exercise 8 for MR brain images.
 - 12.10. Repeat Exercise 8 for PET brain images.
 - 12.11. Register an MR brain image data set with a PET image data set of the same patient as identified in the MATLAB image database. After registration, segment the corresponding cross-section images of the registered MR and PET data sets. Use boundary detection methods to outline the ventricles and skull regions in all images. Superimpose the respective registered, segmented MR and PET images using different colors. Are the boundary segments from the respective MR and PET images aligned with each other? Comment on the registration of MR PET images with the analysis of respective boundary segment alignment.

12.7. REFERENCES

1. H. Damasio and R. Frank, "Three-dimensional in vivo mapping of brain lesions in humans," *Arch. Neurol.*, Vol. 49, pp. 137–143, 1992.
2. P.E. Roland and K. Ziles, "Brain atlases—A new research tool," *Trends Neurosci.*, Vol. 17, pp. 15–24, 1994.
3. M. Sonka, S.K. Tadikonda, and S.M. Collins, "Knowledge-based interpretation of MR brain images," *IEEE Trans. Med. Imaging*, Vol. 15, pp. 443–452, 1996.
4. K.R. Smith, K. Joarder, R.D. Bucholtz, and K.R. Smith, "Multimodality image analysis and display methods for improved tumor localization in stereotactic neurosurgery," *Proc. Annu. Int. Conf. IEEE EMBS*, Vol. 13, No. 1, p. 210, 1991.
5. A.C. Evans, C. Bell, S. Marrett, C.J. Thomson, and A. Hakim, "Anatomical-functional correlation using an adjustable MRI-based region of interest atlas with positron emission tomography," *J. Cereb. Blood Flow Metab.*, Vol. 8, No. 4, pp. 513–530, 1988.

6. A.C. Evans, S. Marrett, J. Torrscorzo, S. Ku, and L. Collins, "MRI-PET correlation in three dimensions using a volume-of-interest (VOI) atlas," *J. Cereb. Blood Flow Metab.*, Vol. 11, No. 1, pp. A69–A78, 1991.
7. M. Bergstrom, J. Boethius, L. Erikson, T. Greitz, T. Ribble, and L. Widen, "Head fixation device for reproducible position alignment in transmission CT and positron emission tomography," *J. Comput. Assist. Tomogr.*, Vol. 5, pp. 136–141, 1981.
8. P.T. Fox, J.S. Perlmuter, and M.E. Raichle, "A stereotactic method of anatomical localization for positron emission tomography," *J. Comput. Assist. Tomogr.*, Vol. 9, No. 1, pp. 141–153, 1985.
9. V. Bettinardi, R. Scardaoni, M.C. Gilardi, G. Rizzo, D. Perani, G. Striano, F. Triulzi, and F. Fazio, "Head holder for PET, CT, and MR studies," *J. Comput. Assist. Tomogr.*, Vol. 15, No. 5, pp. 886–892, 1991.
10. A.V. Levy, J.D. Brodie, J.A.G. Russell, N. D. Volkow, E. Laska, and A.P. Wolf, "The metabolic centroid method for PET brain image analysis," *J. Cereb. Blood Flow Metab.*, Vol. 9, pp. 388–397, 1989.
11. A.V. Levy, E. Laska, J.D. Brodie, N.D. Volkow, and A.P. Wolf, "The spectral signature method for the analysis of PET brain images," *J. Cereb. Blood Flow Metab.*, Vol. 11, pp. A103-A113, 1991.
12. N.M. Alpert, J.F. Bradshaw, D. Kennedy, and J.A. Correia, "The principal axes transformation: A method for image registration," *J. Nucl. Med.*, Vol. 31, No. 10, pp. 1717–1722, 1990.
13. A.V. Levy and D. Warrier, "A new composite phantom for accuracy testing of PET-MRI registration," Brookhaven National Laboratory Interim Report, Chemistry Dept., May 1992.
14. L.K. Arata, A.P. Dhawan, J.P. Broderick, M.F. Gaskil-Shipley, A. V. Levy, and N. D. Volkow, "Three-dimensional anatomical model-based segmentation of MR brain images through principal axes registration," *IEEE Trans. Biomed. Eng.*, Vol. 42, No. 11, pp. 1069–1078, 1995.
15. A.P. Dhawan, L.K. Arata, A.V. Levy, and J. Mentil, "Iterative principal axes registration method for analysis of MR-PET brain images," *IEEE Trans. Biomed. Eng.*, Vol. 42, No. 11, pp. 1079–1087, 1995.
16. C.A. Pelizzari, G.T.Y. Chen, D.R. Spelbring, R.R. Weichselbaum, and C. T. Chen, "Accurate three-dimensional registration of CT, PET and/or MR images of the brain," *J. Comput. Assist. Tomogr.*, Vol. 13, No. 1, pp. 20–26, 1989.
17. D.N. Levin, C.A. Pelizzari, G.T.Y. Chen, C.T. Chen, and M.D. Cooper, "Retrospective geometric correlation of MR, CT, and PET images," *Radiology*, Vol. 169, pp. 601–611, 1988.
18. P. Thomson and A.W. Toga, "A surface based technique for warping three-dimensional images of the brain," *IEEE Trans. Med. Imaging*, Vol. 15, pp. 402–417, 1996.
19. C.A. Davatzikos, J.L. Prince, and R.N. Bryan, "Image registration based on boundary mapping," *IEEE Trans. Med. Imaging*, Vol. 15, pp. 112–115, 1996.
20. A. Toga, *Brain Warping*, Academic Publishers, San Diego, CA, 1999.
21. S.P. Raya and J.K. Udupa, "Shape-based interpolation of multi-dimensional objects," *IEEE Trans. Med. Imaging*, Vol. 9, No. 1, pp. 32–42, 1990.
22. H. Goldstein, *Classical Mechanics*, Addison-Wesley, Reading, MA, 1980.
23. J.C. Gee, L. LeBriquer, C. Barillot, and D.R. Haynor, "Probabilistic matching of brain images," Tech. Rep. IRCS Report 95-07, The Institute for Research in Cognitive Science, April 1995.
24. J.C. Gee, L. LeBriquer, C. Barillot, D.R. Haynor, and R. Bajcsy, "Bayesian approach to the brain image matching problem," Tech Rep. IRCS Report 95-08, The Institute for Research in Cognitive Science, April 1995.
25. R. Bajcsy and S. Kovacic, "Multiresolution elastic matching," *Comput. Vis. Graph. Image Process.*, Vol. 46, No. 1, pp. 1–21, 1989.
26. D.L. Collins, T.M. Peters, and A.C. Evans, "An automated 3D non-linear image deformation procedure for determination of gross morphometric variability in human brain," *Visualization Biomed. Comput.*, SPIE Proceedings, Vol. 2359, SPIE Press, Bellingham, WA, pp. 180–190, 1994.
27. D. Terzopoulos and K. Fleischer, "Modelling inelastic deformation: Viscoelasticity, plasticity fracture," *Comput. Graph.*, Vol. 22, No. 4, pp. 269–278, 1988.
28. R. Dann, J. Holford, S. Kovacic, M. Reivich, and R. Bajcsy, "Three dimensional computerized brain atlas for elastic matching: Creation, initial evaluation," *Proc. SPIE*, Vol. 914, pp. 600–612, 1988.
29. J.C. Gee, M. Reivich, L. Bilaniuk, D. Hackney, and R. Zimmerman, "Evaluation of multiresolution elastic matching using MRI data," *Med. Imaging V: Image Process.*, Vol. 1445, pp. 226–234, 1991.

30. M.I. Miller, G.E. Christensen, Y. Amit, and U. Gerander, "Mathematical textbook of deformable neuroanatomies," *Proc. Natl. Acad. Sci. USA*, Vol. 90, pp. 11944–11948, 1993.
31. K.J. Friston, J. Ashburner, C.D. Frith, J.B. Poline, J.D. Heather, and R.S.J. Frackowiak, "Spatial registration, normalization of images," *Hum. Brain Mapp.*, Vol. 2, pp. 1–25, 1995.
32. Y. Gem, M. Fitzpatrick, B.M. Dawant, J. Bao, R.M. Kessler, and R. A. Margolin, "Accurate localization of cortical convolution in MR brain images," *IEEE Trans. Med. Imaging*, Vol. 15, pp. 418–428, 1996.
33. M. Ferrant, A. Nabavi, B. Macq, F.A. Jolsez, R. Kikinis, and S.K. Warfield, "Registration of 3-D intraoperative MR images of the brain using a finite element biomechanical model," *IEEE Trans. Med. Imaging*, Vol. 20, pp. 1384–1297, 2001.
34. K. Rohr, H.S. Stiehl, R. Sprengel, T.M. Buzug, J. Wesse, and M. H. Kahn, "Landmark based elastic registration using approximating thin-plate splines," *IEEE Trans. Med. Imaging*, Vol. 20, pp. 526–534, 2001.
35. G.E. Christensen and H.J. Johnson, "Consistent image registration," *IEEE Trans. Med. Imaging*, Vol. 20, pp. 568–582, 2001.
36. J. Park, A.A. Young, and L. Axel, "Deformable models with parameter functions for cardiac motion analysis from tagged MRI data," *IEEE Trans. Med. Imaging*, Vol. 15, pp. 278–289, 1996.
37. R.J. Althof, M.G.J. Wind, and J.T. Dobbins, "A rapid automatic image registration algorithm with subpixel accuracy," *IEEE Trans. Med. Imaging*, Vol. 16, pp. 308–316, 1997.
38. Y. Sato, M. Nakamoto, Y. Tamaki, T. Sasama, I. Sakita, Y. Nakajima, M. Monden, and S. Tamura, "Image guidance of breast cancer surgery using 3-D ultrasound images and augmented reality visualization," *IEEE Trans. Med. Imaging*, Vol. 17, pp. 681–693, 1998.
39. J.L. Herring, B.M. Dawant, C.R. Maurer, D.M. Muratore, R.L. Galloway, and J.M. Fitzpatrick, "Surface-based registration of CT images to physical space for image guided surgery of the spine," *IEEE Trans. Med. Imaging*, Vol. 17, pp. 743–752, 1998.
40. I. Bricault, G. Ferretti, and P. Cinquin, "Registration of real and CT derived virtual bronchoscopic images to assist transbronchial biopsy," *IEEE Trans. Med. Imaging*, Vol. 17, pp. 703–714, 1998.
41. J.M. Fitzpatrick, D.G. Hill, and C.R. Maurer, "Image registration," in M. Sonka and J.M. Fitzpatrick (Eds), *Handbook of Medical Imaging, Volume 2: Medical Image Processing and Analysis*, SPIE Press, Bellingham, 2000, pp. 447–514.
42. C.R. Maurer, G.B. Aboutanos, B.M. Dawant, R.J. Maciunas, and J. M. Fitzpatrick, "Registration of 3-D images using weighted geometrical features," *IEEE Trans. Med. Imaging*, Vol. 15, pp. 836–849, 1996.